The 9th European Congress on Computational Methods in Applied Sciences and Engineering
ECCOMAS Congress 2024
3–7 June 2024, Lisboa, Portugal

DROPLET AND PARTICLE FORMATION IN AN X-MICRODEVICE

ALESSANDRO MARIOTTI[1], SARA TOMASI MASONI[1], CHIARA GALLETTI[1], MARIA VITTORIA SALVETTI[1] AND ELISABETTA BRUNAZZI[1]

[1] Department of Civil and Industrial Engineering, University of Pisa
Largo Lucio Lazzarino, 2, 56122 Pisa, Italy
e-mail: alessandro.mariotti@unipi.it

Key words: Microdroplets, nanoparticles, X-microdevice, Computational Fluid Dynamics, microfluidic experiments

Summary. Micro- and nano- droplets and particles find diverse applications in fields such as biology, biotechnology, and pharmaceuticals. They can be fabricated using a variety of materials, both organic and inorganic, and employing various techniques. In particular, these particles are utilized for drug delivery, enabling the transport of Active Pharmaceutical Ingredients (APIs) within the human body. Achieving precise control over the shape, composition, and size of nanoparticles is crucial for such applications. Recent advances in microfluidics have played a key role in ensuring an accurate control of particle quality and many device geometries have been proposed in the literature to achieve well-controlled droplet generation, including the T- and X-shaped junctions used, e.g., for hydrodynamic flow focusing or co-axial injection. In this study, we explore the capabilities of numerical simulations for the computation of droplet and particle formation in microfluidic devices, drawing comparisons with experimental results. Specifically, we employ an X-junction to generate (i) alginate droplets using the segmented dispersed phase method and (ii) chitosan nanoparticles via solvent displacement method. Numerical simulations satisfactorily agree with experiments for all the considered flow rates. Thus, they are demonstrated to be effectively useful in evaluating how different flow regimes occur inside the microdevice as a function of the inlet flow rates and how these, in turn, impact the size and distribution of droplets and particles.

1 INTRODUCTION

Micro and nanoparticles are extensively utilized in various field, including biological, biotechnological, and pharmaceutical fields, due to their versatility in being synthesized from diverse materials [1] and through multiple production techniques [2, 3, 4, 5]. Among these materials, natural polymers are particularly appealing for drug delivery applications because of their inherent biodegradability and biocompatibility. In the present work, we focus on the generation of alginate droplets and chitosan nanoparticles. Sodium alginate is a linear polysaccharide derived from brown algae and chitosan is a linear polysaccharide obtained by deacetylation of chitin, a natural polysaccharide. For many applications, e.g. the pharmaceutical ones, precise control over the size and polydispersity of particles is crucial, as these parameters significantly influence the efficacy and safety of drug delivery systems. The microfluidic approach offers a robust solu-

tion for fabricating nanoparticles and nano/microdroplets, providing excellent control over the synthesis process and enabling the production of high-quality particles for pharmaceutical use [4, 6, 7].

The microfluidic method includes various techniques to produce particles and droplets, depending on the miscibility or immiscibility of the two phases involved. The pinching process, or segmentation of the dispersed phase, involves two immiscible phases, one continuous and one dispersed. The droplet originates from fluid instabilities at the junction of a microdevice, where the two phases come into contact. Here, destabilizing forces, such as interfacial forces, promote droplet formation, while stabilizing forces, including inertial and viscous forces, support jet extension. The ratio between these forces determines the flow regimes within the microdevice. On the other hand, the solvent displacement technique, or nanoprecipitation, involves a solvent containing a solute, which is the raw material for the particles, and an antisolvent in which the solvent is miscible, but the solute is not. When a significant amount of the antisolvent is introduced, the solution undergoes phase separation, leading to the formation of solute particles. In the case of chitosan nanoparticles, the transition to pH higher than 6.5 triggers the precipitation of chitosan and thus the formation of nanoparticles. This process is critical for generating nanoparticles with precise size control and uniformity, essential for advanced pharmaceutical applications.

This work aims at investigating, both experimentally and numerically, the effect of the flow regimes inside the microdevice on the formation of particles and droplets. Indeed, we want assess whether numerical simulations can predict the flow regimes inside the microdevice, as well as the size and size distribution of droplets and particles. To this purpose, we produce alginate dropltes through segmentation and chitosan nanoparticles via nanoprecipitation, thus covering two different generation methods. We employ an X-microdevice operating in a flow-focusing configuration.

2 EXPERIMENTAL METHOD

The X-microdevice is made of three sealed layers of polymethylmethacrylate (PMMA), with the central layer (1 mm thick) having an X-shape cut. The device has four identical channels with a square cross-section of 1 mm, giving a the hydraulic diameter is $d = 1$ mm. Each channel is $L = 60$ mm long. The microdevice is the same as the one used in the experiments by Antognoli et al. [8] and Tomasi Masoni et al. [9, 10]. The X-microdevice is used with three inlets and one outlet configuration.

For the alginate droplets, the two opposite inlet channels are fed with the continuous phase, which is sunflower oil with 0.5 wt% of Span80 surfactant (by Sigma Aldrich). The other inlet channel is fed with the dispersed phase made by dissolving 2 wt% of alginate (by Sigma Aldrich) in deionized water. The dispersed phase is colored with a red food dye (E-124) to distinguish the two inlet streams. To produce chitosan nanoparticles, the two opposite channels are fed with the antisolvent which is a aqueous solution of 1.5 M of sodium acetate. The pH is 9.3. The solvent is fed into the other inlet channel and contains 1.6 mL of acetic acid, 0.35 g of sodium acetate, and a quantity of bidistillated water to obtain 1 L of solution. Then, we add 2.5 g/L of chitosan powder in the solvent. The pH of the solvent is equal to 4.2. The nanoprecipitation mechanism depends on solubility of the chitosan which in turn depends on the pH. To achieve the precipitation of chitosan nanoparticles it is necessary that the mixture of the solvent and

antisolvent has a pH> 6.5. Consequently, a precise control over the pH is crucial for the process. The physical properties of the solutions, i.e., the density ρ and the viscosity μ, are summarized in Tab. 1. For the alginate droplets, the surface tension is 20 mN/m, and the contact angle between the interface and the solid wall is equal to 45°.

The continuous phase and the antisolvent solution are introduced into the device by using two Becton Dickson plastic syringes of 50 mL with the KD Scientific syringe pump Gemini 88. The dispersed phase and the solvent are fed with a Becton Dickson plastic syringe of 20 mL and a Harward Apparatus syringe pump.

Table 1: Physical properties of the solutions at 20°C.

Solution	ρ [kg/m^3]	μ [mPa·s]
Dispersed phase	1008	241
Continuous phase	913	79.5
Solvent	970	5.10
Antisolvent	1042	1.55

The flow inside the microdevice is observed with an upright microscope (Eclipse 80 by Nikon), equipped with a 4× magnifying lens with $N.A. = 0.13$. Images are captured by a high-speed camera (Velociraptor HS by Optomotive), which has a square monochrome sensor of 2048×2048 pixels that allows a maximum frame rate of 174 frames/s. For the experiments, a resolution of 500×2048 pixels and 100 frames/s is chosen.

3 NUMERICAL MODEL

Alginate droplet formation process is investigated through unsteady laminar simulations, performed using the finite-volume commercial-code ANSYS Fluent 2020 R2. The interfacial flow is solved through the Volume Of Fluid (VOF) approach. The domain is reduced to one-quarter of the geometry due to the double-mirror symmetry of the X-microdevice and of the flow field. The PISO algorithm is used for the pressure-velocity coupling, and second-order accurate schemes are employed for spatial discretization. The volume fraction equation of the VOF model is solved using an explicit time scheme. Simulations are carried out at fixed Courant number (CFL=0.5). The starting grid is fully structured with cubical cells of 30 μm × 30 μm × 30 μm. Since the viscosity of the dispersed phase is higher than that of the continuous phase, satellite droplets are produced behind the main droplet and an adaptive grid refinement based on the gradient of the alginate volumetric fraction performed during the simulations to capture satellites. In particular, an Adaptive Mesh Refinement is performed to refine the grid at the interface between the two phases and coarse the grid when necessary. The boundary conditions consist of no-slip at the channel walls, ambient pressure at the outlet, and uniform velocity at the entrance.

Regarding chitosan nanoparticles, the two inlet solutions are completely miscible and steady laminar simulations are carried out with the same finite-volume code. A second-order accurate schemes are used for the spatial discretization, and the SIMPLE algorithm is used for the pres-

sure–velocity coupling. The boundary conditions consist of uniform velocity and concentration of the solutions at the entrance, no-slip velocity at the channel walls, and ambient pressure at the outlet. After preliminary grid-independence analysis, the computational grid is a fully structured grid with $1.62 \cdot 10^6$ cells, with 30 μm $\times$ 30 μm square cells in the cross-section of the channels. The cells are cubical at the confluence region, while they elongate along the inlet and the outlet channels.

4 RESULTS FOR ALGINATE DROPLETS FORMATION

First, we analyze the alginate droplet formation, which occurs in three stages: filling, necking, and pinching-off. Figure 1 represents a typical alginate droplet formation process over the time, visualized during the experiments. A droplet-formation cycle of period τ=1.10 s is considered. The alginate aqueous solution fills the confluence region and stretches into the outlet channel forming a liquid thread. Then the incoming oil causes the necking of the thread of the alginate solution. During the pinch-off phase a main droplet and eventually satellites are produced and driven downstream in the outlet channel. The formation of satellites depends on the viscosity difference between the dispersed and the continuous phases. In fact, when the viscosity of the dispersed phase is larger than the viscosity of the continuous phase, the dispersed phase tends to maintain the liquid thread. Then, when the thread breaks, generates a cascade of satellite drops, which are not desiderable. It should be noted that the instants illustrated in Fig. 1 are not equally spaced in time; indeed, the first stage occurs over a longer timescale compared to the pinch-off phase, which is very rapid.

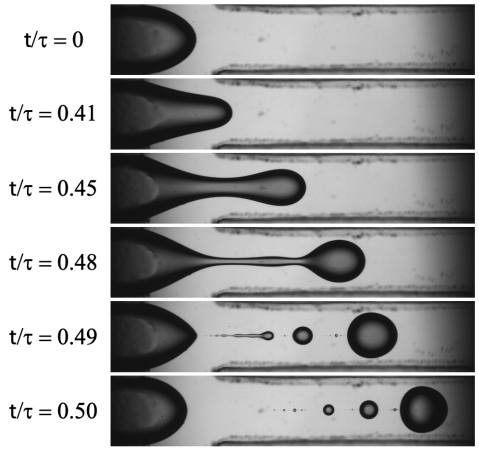

Figure 1: Alginate droplet formation: instantaneous experimental images at different moments during a period τ= 1.10 s. The continuous phase flow rate is 800 μL/min and the dispersed phase flow rate is 10 μL/min.

Figure 2 shows the comparison between experimental flow visualizations and numerical simulations for the production of alginate droplets at a fixed time during the droplet-formation cycle. We considered two cases at the same flow rate ratio ($FRR = Q_C/Q_D = 80$), i.e., 400 μL/min for the oil and 5 μL/min for dispersed phase, and 800 μL/min for the oil and 10 μL/min for the dispersed phase. The agreement is very satisfactory for both the considered cases. By increasing the flow rates (Figs. 2b and 2d), the main droplet decreases in size, but the number

and the dimension of the satellites increase. Indeed, as the continuous phase flow rate increases, the detachment of the droplet takes place further downstream in the outlet channel, thus, the liquid thread is thicker and longer, leading to bigger and more satellites. For a fixed $FRR = 80$, lower flow rates lead to a higher efficiency, resulting in a larger amount of alginate that goes into the main droplet. On the contrary, some alginate is lost in the satellite droplets at flow rates 800 μL/min for the oil and 10 μL/min for the dispersed phase.

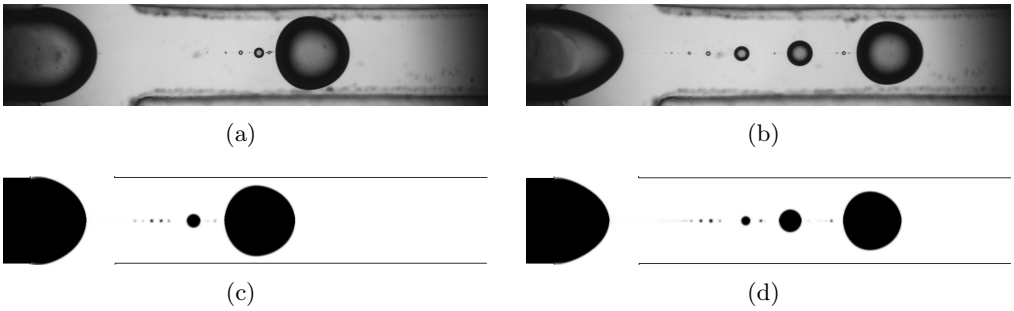

Figure 2: Comparison between (a,b) experimental visualizations and (c,d) numerical simulations of alginate droplets. Results at different flow rates: (a,c) 400 μL/min for the oil and 5 μL/min for the dispersed phase; (b,d) 800 μL/min for the oil and 10 μL/min for the dispersed phase.

5 RESULTS FOR CHITOSAN NANOPARTICLES PRODUCTION

Regarding the chitosan nanoparticles production, we first focus on the capability of numerical simulations to predict the flow regimes inside the device, which is essential for particle precipitation. In fact, the flow field inside the device affect the particle production, both in terms of size and size distribution of the particles. Figure 3 shows the comparison between experimental and numerical results. The experimental flow visualzation are obtained thanks to the difference between the refractive index of the two inlet streams. Therefore, the optical rays are somewhat diverted in their course across the specimen due to refraction resulting from the refractive index differences between the two solutions. Consequently, at the contact fronts of the two different fluids, darker or brighter streaks compared to the rest of the image, can be observed. Following the procedure described in [11], proper adjustments of the condenser and the field diaphragms, allowed us to deliberately highlight the streaks. In this way streaks are exploited to visualize the flow topology and vortical structures. The mass fraction of the solvent and the isosurfaces of the λ_2 vortex-indicator are evaluated from numerical simulations. The λ_2 method is an algorithm that adequately detect the vortices from a three-dimensional fluid velocity field.

Based on the experimental flow visualizations, three different flow regimes occur in the X-microdevice. We analyze herein three different combination of flow rates, that represent the three flow regimes. In particular, we consider in Fig. 3a an outlet flow rate Q equal to 10 mL/min with a ratio between the antisolvent and the solvent flow rate R equal to 10, in Fig. 3b Q=20 mL/min and R=25, and in Fig. 3c Q=50 mL/min and R=50.

At a low outlet flow rate, as shown in Fig. 3a-c, the hydrodynamic flow focusing regime occurs, characterized by the confinement of the solvent flow in a region located at the center of the outlet channel. There is a perfect match between the contact area of the solvent and antisolvent

in experiments (Fig. 3a) and the relative mass fractions in simulations (Fig. 3b). No vortical structures are detected (Fig. 3c). It is worth noting that by selecting the solvent/antisolvent flow rates, it is possible to control the width of the flow focusing region, which is a crucial parameter in determining the size of the particles. By increasing the outlet flow rate, Q, vortical structures begin to form in the confluence region in a transitional regime (Fig. 3d-f). Finally, two U-shaped counter-rotating vortical structures are present at the highest flow rate in the vortex regime. The vortices lead to a "mushroom" structure in experimental flow visualizations (Fig. 3g). Again, the solvent mass fractions in the simulations (Fig. 3h) match the experimental results very well. We also note good agreement between simulations and experiments in predicting the flow rate at which the three regimes occur. The correct evaluation of the flow pattern will allow the implementation of a precipitation law in numerical simulations to determine the final size distribution of the nanoparticles in future investigations. Preliminary experimental evidence (Zetasizer analysis) shows that we can produce monodisperse particles in the hydrodynamic flow focusing regime, as they precipitate and grow in a well-defined and straight contact area between the solvent and antisolvent. On the other hand, in the vortex regime, the contact area between the two inlet streams is not well-defined, and the mixing of the flow is more pronounced due to the vortical structures, leading to a more widespread size distribution of the nanoparticles.

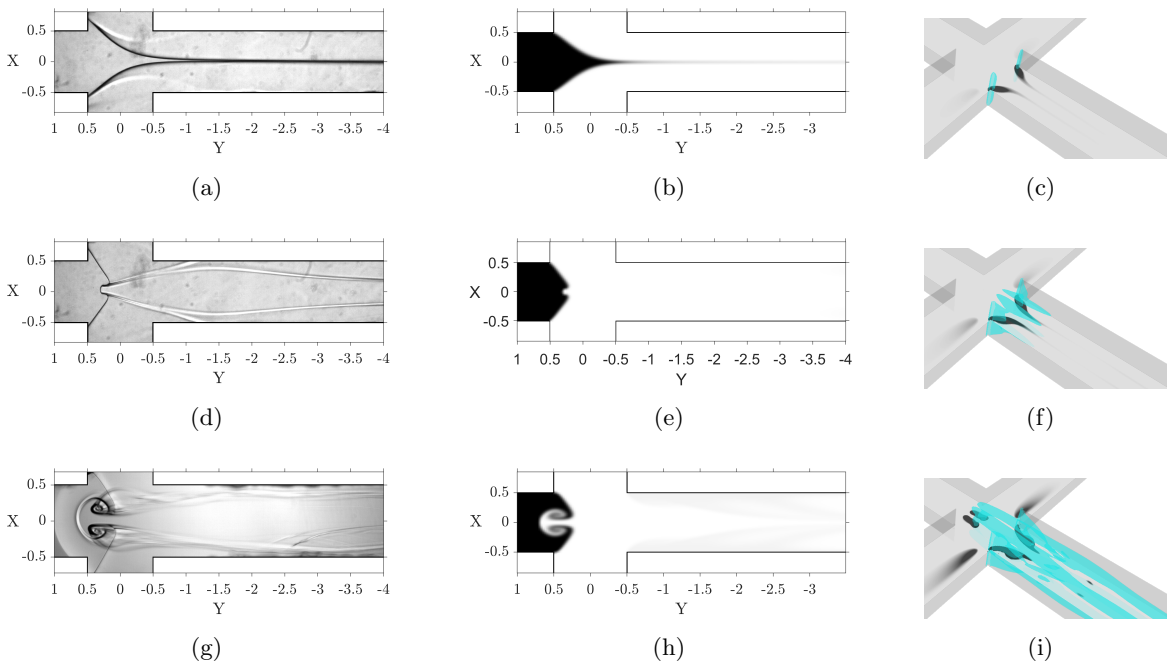

Figure 3: Production of chitosan nanoparticles. (a,d,g) Experimental visualization of the contact area between the solvent and the antisolvent. (b,e,h) Solvent mass fraction (black) in numerical simulations. (c,f,i) Isosurfaces of the λ_2 vortex-indicator evaluated from numerical simulations. Considered flow rates for solvent and antisolvent: (a-c) 0.91 mL/min and 9.09 mL/min; (d-f) 0.77 mL/min and 19.23 mL/min; (g-i) 0.98 mL/min and 49.02 mL/min (e-f).

6 CONCLUSIONS

In the present work, alginate microdroplets and chitosan nanoparticles are produced in an X-microdevice operating with three inlets and one outlet. The alginate droplets are produced through the segmentation of the dispersed phase method, whereas the chitosan nanoparticles are obtained through precipitation.

Regarding alginate microdroplets, we found that for a fixed flow rate ratio, the quality of the microdroplets can be improved by reducing both the oil and alginate flow rates. Indeed, almost all of the alginate is encapsulated in the main droplet without the formation of satellites. However, the total production of droplets for a single device is reduced. To improve production without a significant loss of efficiency, we can increase only the alginate flow rate.

Chitosan nanoparticles are obtained using the same device. Three different regimes are identified in experiments: flow focusing, transition, and vortex. Monodisperse nanoparticles are produced in the flow focusing regime. In contrast, the vortex regime generates larger and more polydisperse nanoparticles. Numerical simulations accurately predict the flow regimes, and future studies will be devoted to modeling the nucleation and precipitation mechanisms in the CFD simulations.

REFERENCES

[1] Campos, E., Branquinho, J., Carreira, A. S., Carvalho, A., Coimbra, P., Ferreira, P., Gil, M. H., 2013. "Designing polymeric microparticles for biomedical and industrial applications." European Polymer Journal 49, no. 8: 2005-2021. http://doi.org/10.1016/j.eurpolymj.2013.04.033

[2] Capretto, L., Carugo, D., Mazzitelli, S., Nastruzzi, C., Zhang, X., 2013. "Microfluidic and lab-on-a-chip preparation routes for organic nanoparticles and vesicular systems for nanomedicine applications." Advanced Drug Delivery Reviews 65, no. 11: 1496-1532. http://doi.org/10.1016/j.addr.2013.08.002

[3] Carvalho, J. P. F., Silva, A. C. Q., Silvestre, A. J. D., Freire, C. S. R., and Vilela, C., 2021. "Spherical Cellulose Micro and Nanoparticles: A Review of Recent Developments and Applications." Nanomaterials 11, no. 10: 2744. http://doi.org/10.3390/nano11102744

[4] Carvalho, B. G., Ceccato, B. T., Michelon, M., Han, S. W., de la Torre, L. G., 2022. "Advanced Microfluidic Technologies for Lipid Nano-Microsystems from Synthesis to Biological Application." Pharmaceutics 14, no. 1: 141. http://doi.org/10.3390/pharmaceutics14010141

[5] Liu, Z., Fontana, F., Python, A., Hirvonen, J. T., Santos, H. A., 2020. "Microfluidics for Production of Particles: Mechanism, Methodology, and Applications." Small 16, no. 9: 1904673. http://doi.org/10.1002/smll.201904673

[6] Cetin, B., Asik, M. D., Taze, S., 2014. "Design and Fabrication of a Microfluidic Device for Synthesis of Chitosan Nanoparticles." Journal of Nanotechnology in Engineering and Medicine 4, no. 3: 031004. http://doi.org/10.1115/1.4026287

[7] Zhu, P., Wang, L., 2017. "Passive and active droplet generation with microfluidics: a review." Lab Chip 17, no. 1: 34-75. http://doi.org/10.1039/C6LC01018K

[8] Antognoli, M., Tomasi Masoni, S., Mariotti, A., Mauri, R., Brunazzi, E., Galletti, C., 2022. "Investigation on steady regimes in a X-shaped micromixer fed with water and ethanol." Chemical Engineering Science 248: 117254. http://doi.org/10.1016/j.ces.2021.117254

[9] Tomasi Masoni, S., Antognoli, M., Mariotti, A., Mauri, R., Salvetti, M. V., Galletti, C., Brunazzi, E., 2022. "Flow regimes, mixing and reaction yield of a mixture in an X-microreactor." Chemical Engineering Journal 437: 135113. http://doi.org/10.1016/j.cej.2022.135113

[10] Tomasi Masoni, S., Mariotti, A., Antognoli, M., Galletti, C., Mauri, R., Salvetti, M. V., Brunazzi, E., 2024. "Prediction of the reaction yield in a X-micromixer given the mixing degree and the kinetic constant." Physical Review Fluids 9: 024202. http://doi.org/10.1103/PhysRevFluids.9.024202

[11] Mariotti, A., Antognoli, M., Galletti, C., Mauri, R., Salvetti, M. V., Brunazzi, E., 2020. "The role of flow features and chemical kinetics on the reaction yield in a T-shaped micro-reactor." Chemical Engineering Journal 396: 125223. http://doi.org/10.1016/j.cej.2020.125223